

Charge trap layer enabled positive tunable V_{fb} in β -Ga₂O₃ gate stacks for enhancement mode transistors

Dipankar Biswas,¹ Chandan Joishi,^{1,2} Jayeeta Biswas,¹ Prabhans Tiwari,¹
and Saurabh Lodha^{1,a}

*1)Department of Electrical Engineering, Indian Institute of Technology Bombay,
Mumbai, Maharashtra 400076, India*

*2)Department of Electrical and Computer Engineering, The Ohio State University,
Columbus, OH 43210, U.S.A.*

E-mail: slodha@ee.iitb.ac.in

(Dated: 11 May 2020)

Abstract

β -Ga₂O₃ based enhancement mode transistor designs are critical for the realization of low loss, high efficiency next generation power devices with rudimentary driving circuits. A novel approach towards attaining a high positive flat band voltage (V_{fb}) of 10.6 V in β -Ga₂O₃ metal-oxide-semiconductor capacitors (MOSCAPs), with the ability to fine tune it between 3.5 V to 10.6 V, using a polycrystalline AlN charge trap layer has been demonstrated. This can enable enhancement mode operation over a wide doping range. Excellent V_{fb} retention of ~97% for 10⁴ s at 55 °C was exhibited by the gate stacks after charge trapping, hence reducing the requirement of frequent charge injection cycles. In addition, low gate leakage current density (J_g) for high negative gate voltages ($V_g \sim -60$ V) indicates the potential of this gate stack to enable superior breakdown characteristics in enhancement mode transistors.

^aTo whom correspondence should be addressed

A high theoretical breakdown field (E_{br}) of 8 MVcm^{-1} resulting from its ultrawide band gap ($E_g=4.8 \text{ eV}$), combined with a reasonable electron mobility ($\mu=300 \text{ cm}^2\text{V}^{-1}\text{s}^{-1}$), enable high figures of merit in power switching for $\beta\text{-Ga}_2\text{O}_3$.^{1,2} In addition, cost effective growth of bulk crystals with low defect density over a wide doping range by scalable melt based methods (Czochralski, float-zone, edge-defined film-fed growth, etc.) has led to significant interest in this material for next generation power electronics.³⁻⁵

Over the years, $\beta\text{-Ga}_2\text{O}_3$ based vertical devices such as Schottky diodes, trench metaloxide-semiconductor field-effect transistors and current aperture vertical electron transistors (CAVETs), as well as lateral devices in the form of metal-semiconductor field-effect transistors (MESFETs), metal-oxide-semiconductor field-effect transistors (MOSFETs) and modulation-doped field-effect transistors (MODFETs) have been demonstrated with promising performance.⁶⁻¹² For lateral FETs, although existing reports show good progress in the development of depletion mode transistors with acceptable ON-state current densities and high breakdown voltages (V_{br}), the lack of p-type doping has limited the advancement of enhancement mode (normally-off) transistors. These are critical for low power and high efficiency next generation high power switches.¹¹⁻¹³ Recently, device design technologies such as recessed-gate, wrap-gate fin arrays, unintentionally doped channels and ferroelectric gate dielectrics have emerged to realize normally-off transistors on $\beta\text{-Ga}_2\text{O}_3$.¹⁴⁻¹⁷ To further increase the current density and make it comparable to existing GaN-based technologies, modulation of higher charge density channels using different gate dielectrics are being explored.¹⁸ Owing to its high dielectric constant (~ 8), reasonable conduction band offset (ΔE_c) of 1.5-1.7 eV and a high quality interface with $\beta\text{-Ga}_2\text{O}_3$, Al_2O_3 has been the current dielectric of choice for $\beta\text{-Ga}_2\text{O}_3$ MOSFETs.¹⁸⁻²⁰ Developing further, we have recently demonstrated an $\text{Al}_2\text{O}_3/\text{SiO}_2$ bi-layer stack to leverage the benefits of both Al_2O_3 (high dielectric constant) and SiO_2 (higher ΔE_c of $\sim 3.6 \text{ eV}$) which enabled a high, positive flat band voltage (V_{fb}) of 3.25 V (in comparison to 0.74 V on using only Al_2O_3).²¹ The higher V_{fb} was attributed to the negative oxide charge in SiO_2 deposited by atomic layer deposition (ALD).²² The idea of utilizing negative gate dielectric charge to realize normally-off transistors is worth exploring in greater detail.

In this letter we realize normally-off operation through the introduction of a charge trap layer to house the negative charge in the gate dielectric stack. We demonstrate high positive

V_{fb} that can be tuned from 3.5 V to 10.6 V (with negligible impact on the dielectric/channel interface) in β -Ga₂O₃ MOSCAPs by controlled electron injection into a polycrystalline AlN charge trap layer sandwiched between Al₂O₃ and SiO₂. Moreover, excellent V_{fb} retention of ~97% for 10⁴ s at 55 °C helps reduce the frequency of charge injection cycles needed to sustain the charge. The introduction of AlN gives an added benefit of reducing the J_g for high negative V_g (~-60 V) compared to an Al₂O₃/SiO₂ bilayer stack. Hence, this stack design is expected to aid realization of normally-off transistors with excellent breakdown characteristics.

To study the morphology of AlN on β -Ga₂O₃ ($\bar{2}01$), 18 nm of the film was deposited by plasma-enhanced ALD (PEALD) using trimethylaluminum (TMA) and ammonia plasma at 200 °C. Grazing-incidence x-ray diffraction (GIXRD) was performed using Cu K α radiation in a Rigaku Smartlab diffractometer. The existence of diffraction peaks corresponding to (100), (101), (102), (110), (103) and (112) planes confirms the presence of hexagonal wurzite phase in polycrystalline AlN as shown in Fig. 1(a).²³ X-ray photoelectron spectroscopy (XPS) analysis of the deposited AlN film (supplementary material) shows the presence of two different peaks in the Al2p spectrum at binding energies of 74.4 eV and 75.6 eV corresponding to Al-N and Al-O bonds, respectively. The presence of AlON is confirmed by the appearance of a sub-peak corresponding to Al-O-N bonds at 398.7 eV along with the main peak at 397.3 eV for Al-N bonds in the N1s spectrum.²⁴ Also, the atomic percentages extracted from the areas under the Al2p, N1s and O1s spectra show a distribution of 39.3%, 35.9% and 24.7% for Al, N and O, respectively. Despite having a similar ΔE_c as that of Al₂O₃ with β -Ga₂O₃ (Fig. 1(b)), the deep energy level states present at the polycrystalline grain boundaries of AlN can serve as effective charge trapping sites.^{24,25}

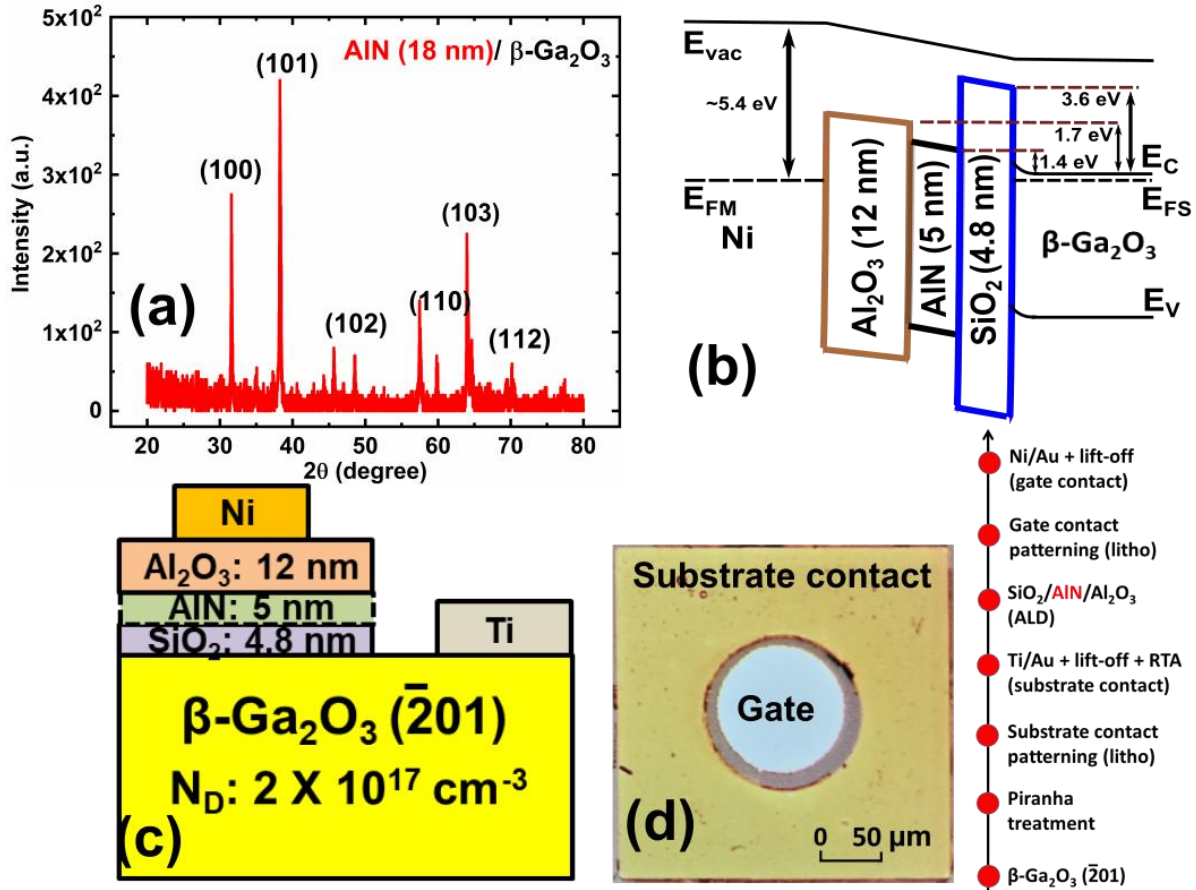


FIG. 1. (a) Grazing incidence x-ray diffraction pattern confirming the formation of polycrystalline AlN on β -Ga₂O₃. (b) Electron energy band diagram of Ni/Al₂O₃/AlN/SiO₂/ β -Ga₂O₃ sample at equilibrium. (c) Cross-section schematic and (d) optical micrograph of fabricated MOSCAPs with a step-wise process flow.

For a comparative study, two 5×5 mm² square samples from the same Sn doped β -Ga₂O₃ ($\bar{2}01$) wafer with a background doping of 2×10^{17} cm⁻³ (Tamura corporation) were used for the fabrication of Ni/Al₂O₃/SiO₂/ β -Ga₂O₃ and Ni/Al₂O₃/AlN/SiO₂/ β -Ga₂O₃ MOSCAPs. The background doping concentration of the substrate was verified by fitting the $1/C^2 - V$ plot (shown in supplementary material) generated from the capacitance-voltage ($C - V$) data. At the start of the fabrication process, the samples were degreased organically by ultrasonication for 3 min each in acetone and methanol followed by a piranha solution (deionised (DI) water:30% H₂O₂:96% H₂SO₄ in 1:1:4 ratio) dip for 5 min. This was done to ensure a high quality SiO₂/ β -Ga₂O₃ interface, as previously reported.²¹ Optical lithography

was used for defining the substrate contact region prior to ohmic metal (Ti/Au) deposition in an electron beam evaporator (EBE) and lift-off. The samples were rapid annealed at a temperature of 470 °C for 1 min in an N₂ atmosphere to lower the contact resistance. This was followed by simultaneous deposition of 4.8 nm thick SiO₂ on both samples by PEALD using tris(dimethylamino)silane and oxygen plasma at 250 °C. The control sample Al₂O₃/SiO₂ was unloaded from the ALD chamber and a 5 nm AlN charge trap layer was deposited on the other sample at 200 °C using TMA and ammonia plasma, before depositing 12 nm Al₂O₃ simultaneously on both samples using TMA and DI water at 250 °C in the same chamber. Thickness and stoichiometry of the gate dielectrics were studied using spectroscopic ellipsometry and XPS, respectively. To confirm the formation of Al₂O₃/AlN/SiO₂ and Al₂O₃/SiO₂ stacks, XPS depth profiles were measured on silicon monitor wafers loaded simultaneously in the ALD chamber during gate dielectric deposition (supplementary material). Next, optical lithography, metal deposition by EBE and lift-off were done to form Ni/Au gate contacts. Finally, the dielectrics were selectively etched from the top of the substrate contacts using a buffered-oxide-etch solution (5:1) after defining etch areas through optical lithography. Figs. 1(c) and (d) show the cross-section schematic and top view (with a step-wise process flow), respectively, of the fabricated MOSCAPs.

Fig. 2(a) shows the $C - V$ characteristics of as-fabricated Ni/Al₂O₃/SiO₂/β-Ga₂O₃ and Ni/Al₂O₃/AlN/SiO₂/β-Ga₂O₃ gate stacks measured using a B1500A semiconductor device analyzer. A peak-to-peak ac signal of 30 mV superimposed on a dc voltage swept at 50 mV/s from depletion to accumulation with an initial hold time of 10 s was used for frequency dependent $C - V$ measurements. Negligible frequency dispersion (supplementary material) combined with steep $C - V$ characteristics indicate a high quality SiO₂/β-Ga₂O₃ interface. Along with an increase in effective oxide thickness (EOT) as seen in the reduced accumulation capacitance (C_{ox}), the incorporation of AlN between Al₂O₃ and SiO₂ reduces the effect of positive oxide charge in Al₂O₃ on β-Ga₂O₃, thus increasing the V_{fb} w.r.t Ni/Al₂O₃/SiO₂/βGa₂O₃. Further, application of a positive voltage stress (charging voltage pulse) above 6 V increases the V_{fb} in both gate stacks (Figs. 2(b) and (c)), attributed to the trapping of electrons injected through the thin SiO₂ interfacial layer into the gate dielectric

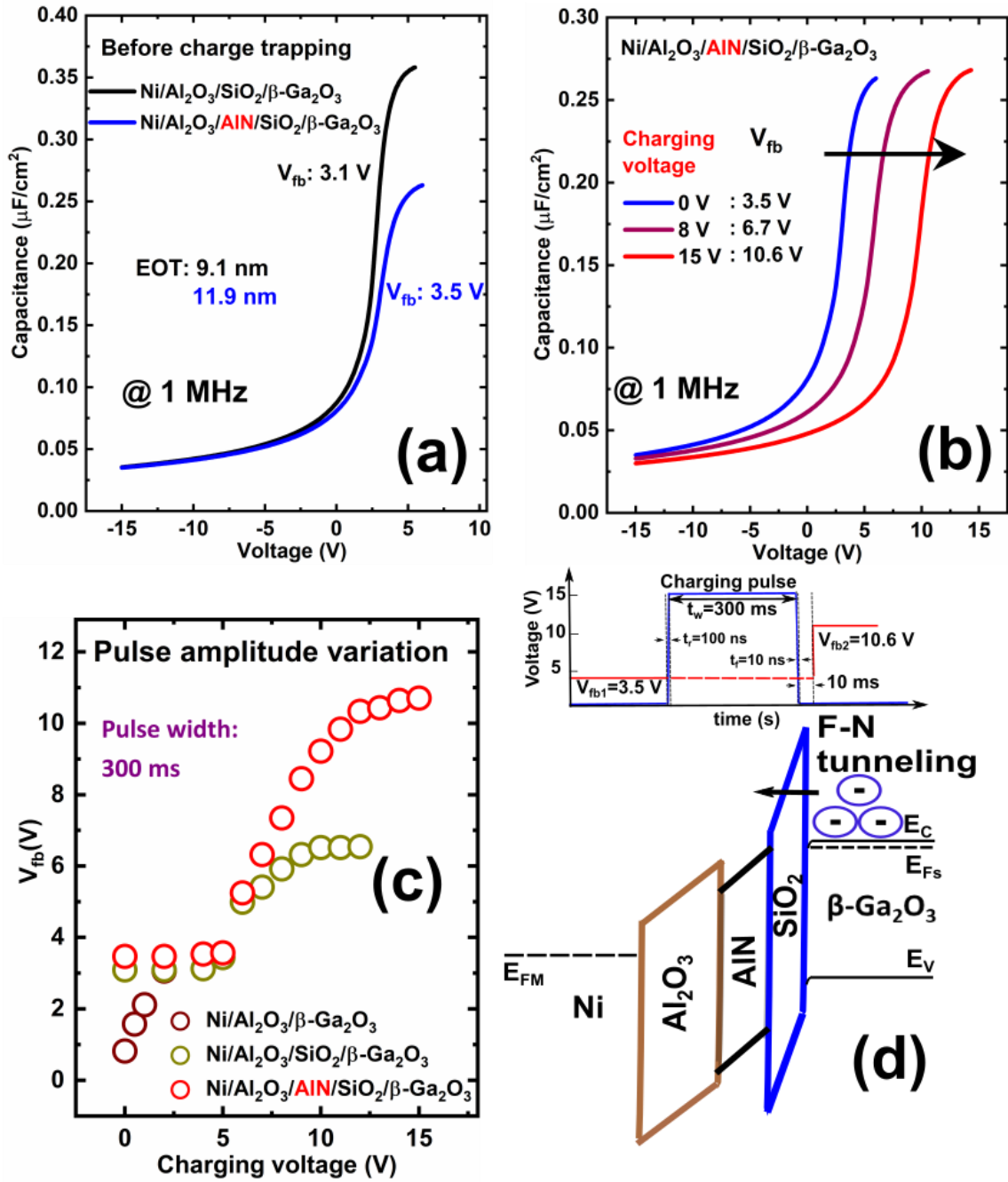


FIG. 2. $C - V$ characteristics of (a) as-fabricated Ni/Al₂O₃/SiO₂/β-Ga₂O₃ and Ni/Al₂O₃/AlN/SiO₂/β-Ga₂O₃ gate stacks before charge trapping, and, (b) Ni/Al₂O₃/AlN/SiO₂/β-Ga₂O₃ gate stack after applying 8 and 15 V charging voltage pulses. (c) V_{fb} tunability with varying amplitude of charging voltage pulse. (d) Electron energy band diagram showing tunneling of electrons into the gate stack under positive voltage stress applied by a pulsed signal (timing diagram shown above).

(AlN or Al₂O₃) by F-N tunneling, as shown in Fig. 2(d). Details about the charge injection process are provided in the supplementary material. For the Ni/Al₂O₃/SiO₂/β-Ga₂O₃ stack, probable sites for electron trapping are located at the Al₂O₃/SiO₂ interface. On the other hand, charge trapping in deep level trap states at the polycrystalline grain boundaries in AlN are likely to be responsible for V_{fb} shifts till 10.6 V in the Ni/Al₂O₃/AlN/SiO₂/β-Ga₂O₃ stack.^{25,26}

The presence of deep level trap states in polycrystalline AlN is supported by the excellent retention of V_{fb} observed in Ni/Al₂O₃/AlN/SiO₂/β-Ga₂O₃ as shown in Figs. 3(a) and (b). After 10⁴ s at 55 °C, a V_{fb} reduction of only 0.3 V (0.1 V at room temperature) was observed in contrast to 2.6 V (0.7 V at room temperature) for Ni/Al₂O₃/SiO₂/β-Ga₂O₃. Hysteresis measurements using bi-directional $C - V$ sweeps were carried out before and after charge trapping (supplementary material) which ruled out the impact of border trap occupancy on V_{fb} tunability. A gradual increase in V_{fb} was observed in Ni/Al₂O₃/β-Ga₂O₃ MOSCAPs also (Fig. 2(c)). This can be attributed to the occupancy of linearly distributed (in space and energy) trap states in Al₂O₃.²⁷ However, very poor V_{fb} retention of 2.2 V at room temperature was observed for the Ni/Al₂O₃/β-Ga₂O₃ stack.

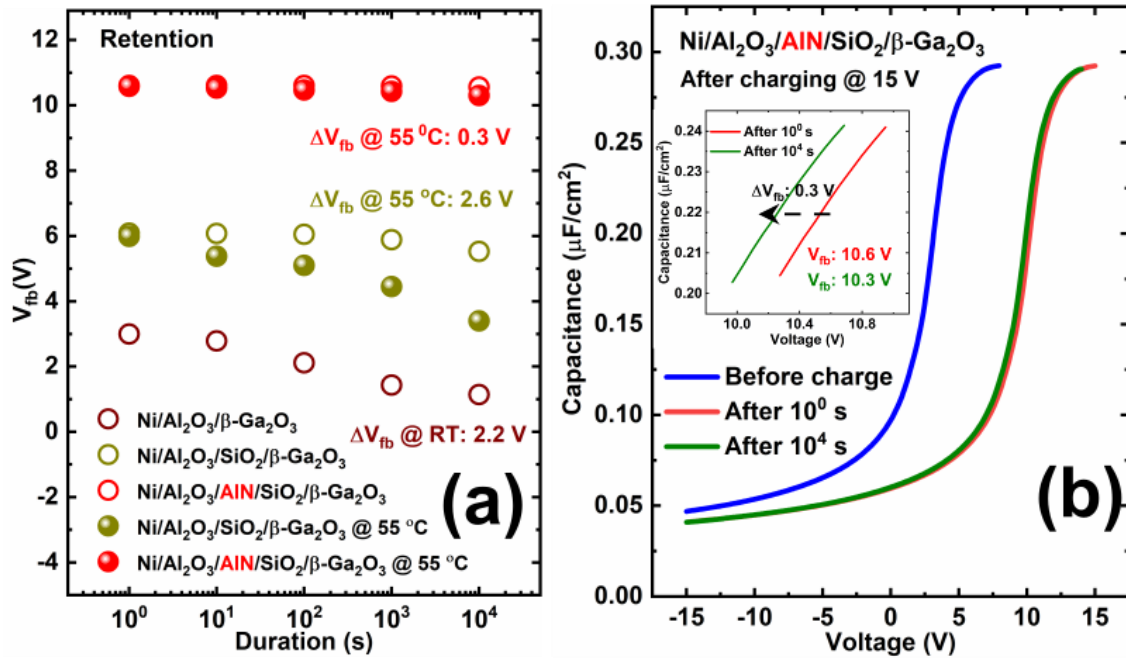


FIG. 3. (a) V_{fb} retention w.r.t time at room temperature and 55 °C for various gate dielectric stacks, and, (b) $C - V$ characteristics of Ni/Al₂O₃/AlN/SiO₂/β-Ga₂O₃ MOSCAP showing the effect of charge trapping on V_{fb} followed by its negligible (~ 0.3 V) reduction after 10⁴ s at 55 °C.

As shown in Figs. 4(a) and (b), nearly the same amount of charge can be modulated before and after charge trapping by both gate stacks throughout their V_{fb} range. Charge values were extracted by integrating the area under their respective $C-V$ curves.

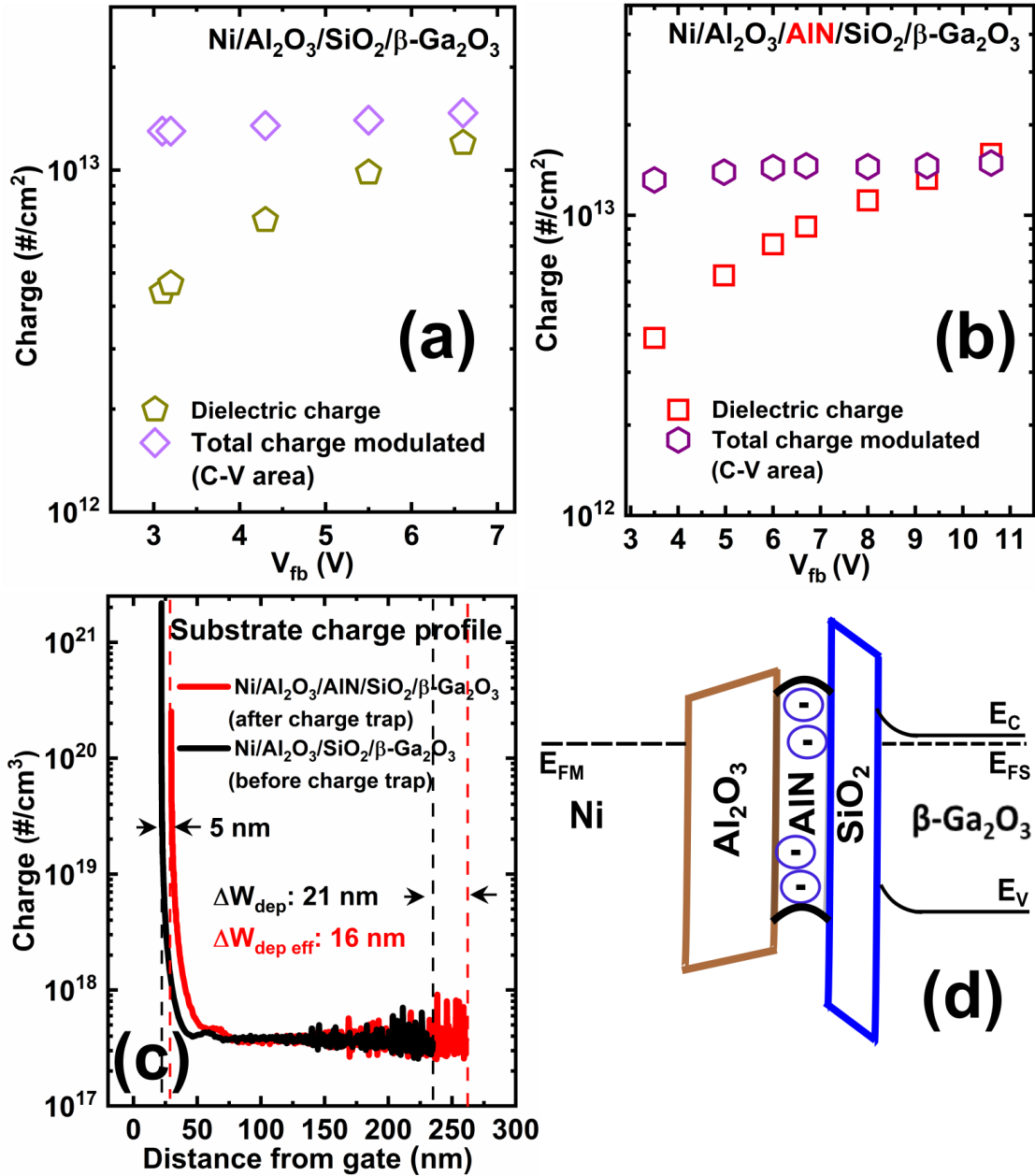


FIG. 4. Plots showing stored dielectric charge and $C-V$ modulated substrate charge densities for (a) Ni/Al₂O₃/SiO₂/β-Ga₂O₃, and, (b) Ni/Al₂O₃/AlN/SiO₂/β-Ga₂O₃ gate stacks. (c) Substrate charge profiles of Ni/Al₂O₃/SiO₂/β-Ga₂O₃ (before charge trapping) and Ni/Al₂O₃/AlN/SiO₂/β-Ga₂O₃ (after charge trapping), and, (d) equilibrium electron energy band diagram of Ni/Al₂O₃/AlN/SiO₂/β-Ga₂O₃ (after charge trapping).

Despite a lower C_{ox} (due to higher EOT) the Ni/Al₂O₃/AlN/SiO₂/β-Ga₂O₃ stack is able to modulate nearly the same amount of charge as the Ni/Al₂O₃/SiO₂/β-Ga₂O₃ stack due to extra substrate charge depletion as observed through the increase in depletion width (Fig. 4(c)). The increase in V_{fb} is due to added negative dielectric charge injected under the application of a positive voltage pulse. The effective dielectric charge density (N_{eff}) was calculated using equation 1 and the V_{fb} value extracted from $C - V$ characteristics,

$$N_{eff} = \frac{C_{ox}|\phi_{MS} - V_{fb}|}{qA} \quad (1)$$

where ϕ_{MS} is the work function difference between the gate metal (Ni) and β-Ga₂O₃, q is unit electric charge and A is the area of the fabricated MOSCAPs.

Reduced gate leakage current density, J_g , for high negative gate voltages exhibited by the Ni/Al₂O₃/AlN/SiO₂/β-Ga₂O₃ capacitor is likely due to better electric field distribution in the dielectric stack in comparison to the Ni/Al₂O₃/SiO₂/β-Ga₂O₃ sample. Higher EOT due to the introduction of AlN in Ni/Al₂O₃/AlN/SiO₂/β-Ga₂O₃ gate stack further helps in reducing J_g for higher negative as well as positive gate voltages in comparison to the Ni/Al₂O₃/SiO₂/β-Ga₂O₃ capacitor. After charge trapping, an increase in J_g for higher negative gate voltages (< -25 V) was seen for the Ni/Al₂O₃/SiO₂/β-Ga₂O₃ sample (Fig. 5(a)). In contrast, the Ni/Al₂O₃/AlN/SiO₂/β-Ga₂O₃ sample demonstrated a consistently low J_g till V_g of ~-60 V before as well as after charge trapping (Fig. 5(b)). Hence, apart from fine tuning V_{fb} for normally-off operation, the charge trap stack is also capable of demonstrating higher breakdown voltages compared to conventional bilayer gate stacks. Table 1 summarizes the positive V_{fb} and V_t values for gate stacks and enhancement mode transistors, respectively, obtained using different material, process and design techniques.

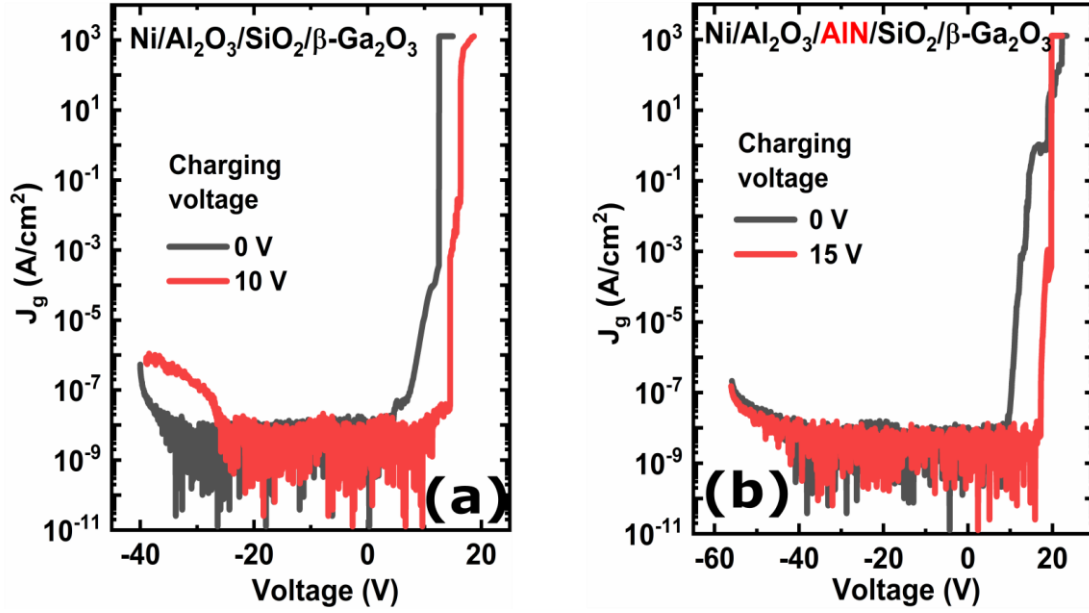


FIG. 5. (a) J_g vs V_g for (a) Ni/Al¹O₃/SiO₂/β-Ga₂O₃, and, (b) Ni/Al₂O₃/AlN/SiO₂/β-Ga₂O₃ gate stacks.

TABLE I. Summary of enhancement mode V_t and V_{fb} values for reported β-Ga₂O₃ MOSFETs and MOSCAPs, respectively.

Ref no.	Method	V_{fb} (V)	V_t (V)
17	Gate recess	-	0
18	Wrap-gate fin FET	-	1
19	UID channel	-	0
20	Ferroelectric charge storage	-	0
21	LPCVD+PDA	3.5	-
21	ALD+FGA	2.5	-
24	Bi-layer dielectric	3.25	-
This work	Charge trap layer	3.5 - 10.6	-

In summary, we demonstrate positive and tunable V_{fb} with superior breakdown properties using a polycrystalline AlN charge trap inter-layer between Al₂O₃ and SiO₂ for enhancement mode β-Ga₂O₃ transistors. Positive V_{fb} ranging from 3.5 V to 10.6 V (3× tunable) was realized without compromising the dielectric/channel interface quality. Excellent V_{fb}

retention of ~97% measured till 10^4 s at 55 °C after charge trapping demonstrates robust gate stack operation with less frequent requirement of charge injection cycles.

See supplementary material for details on extraction of β -Ga₂O₃ doping density, charge trapping mechanism, XPS analyses confirming the formation of AlON along with depth profiles for the Al₂O₃/AlN/SiO₂ and Al₂O₃/SiO₂ stacks.

The authors acknowledge the Ministry of Electronics and Information Technology and Department of Science and Technology, Government of India, for funding this work.

REFERENCES

- ¹B. J. Baliga, Journal of Applied Physics **53**, 1759 (1982), <https://doi.org/10.1063/1.331646>.
- ²H. H. Tippins, Phys. Rev. **140**, A316 (1965).
- ³Y. Oshima, E. G. Vllora, Y. Matsushita, S. Yamamoto, and K. Shimamura, Journal of Applied Physics **118**, 085301 (2015).
- ⁴H. Aida, K. Nishiguchi, H. Takeda, N. Aota, K. Sunakawa, and Y. Yaguchi, Japanese Journal of Applied Physics **47**, 8506 (2008).
- ⁵M.-Y. Tsai, O. Bierwagen, M. E. White, and J. S. Speck, Journal of Vacuum Science & Technology A **28**, 354 (2010).
- ⁶H. Dong, S. Long, H. Sun, X. Zhao, Q. He, Y. Qin, G. Jian, X. Zhou, Y. Yangtong, W. Guo, W. Xiong, W. Hao, Y. Zhang, H. Xue, X. Xiang, Y. Zhaoan, H. Lv, Q. Liu, and M. Liu, IEEE Electron Device Letters **PP**, 1 (2019).
- ⁷M. Wong, K. Goto, H. Murakami, Y. Kumagai, and M. Higashiwaki, IEEE Electron Device Letters **PP**, 1 (2018).
- ⁸K. Konishi, K. Goto, H. Murakami, Y. Kumagai, A. Kuramata, S. Yamakoshi, and M. Higashiwaki, Applied Physics Letters **110**, 103506 (2017), <https://doi.org/10.1063/1.4977857>.
- ⁹W. Li, Z. Hu, K. Nomoto, Z. Zhang, J.-Y. Hsu, Q. T. Thieu, K. Sasaki, A. Kuramata, D. Jena, and H. G. Xing, Applied Physics Letters **113**, 202101 (2018), <https://doi.org/10.1063/1.5052368>.
- ¹⁰C. Joishi, S. Rafique, Z. Xia, L. Han, S. Krishnamoorthy, Y. Zhang, S. Lodha, H. Zhao, and S. Rajan, Applied Physics Express **11**, 031101 (2018).

- ¹¹S. Krishnamoorthy, Z. Xia, C. Joishi, Y. Zhang, J. McGlone, J. Johnson, M. Brenner, A. R. Arehart, J. Hwang, S. Lodha, and S. Rajan, *Applied Physics Letters* **111**, 023502 (2017), <https://doi.org/10.1063/1.4993569>.
- ¹²M. Higashiwaki, K. Sasaki, T. Kamimura, M. Hoi Wong, D. Krishnamurthy, A. Kuramata, T. Masui, and S. Yamakoshi, *Applied Physics Letters* **103**, 123511 (2013), <https://doi.org/10.1063/1.4821858>.
- ¹³K. Zeng, J. Wallace, C. Heimbürger, K. Sasaki, A. Kuramata, T. Masui, J. Gardella, and U. Singiseti, *IEEE Electron Device Letters* **PP**, 1 (2017).
- ¹⁴K. D. Chabak, J. P. McCandless, N. A. Moser, A. J. Green, K. Mahalingam, A. Crespo, N. Hendricks, B. M. Howe, S. E. Tetlak, K. Leedy, R. C. Fitch, D. Wakimoto, K. Sasaki, A. Kuramata, and G. H. Jessen, *IEEE Electron Device Letters* **39**, 67 (2018).
- ¹⁵K. D. Chabak, N. Moser, A. J. Green, D. E. Walker, S. E. Tetlak, E. Heller, A. Crespo, R. Fitch, J. P. McCandless, K. Leedy, M. Baldini, G. Wagner, Z. Galazka, X. Li, and G. Jessen, *Applied Physics Letters* **109**, 213501 (2016), <https://doi.org/10.1063/1.4967931>.
- ¹⁶M. H. Wong, Y. Nakata, A. Kuramata, S. Yamakoshi, and M. Higashiwaki, *Applied Physics Express* **10**, 041101 (2017).
- ¹⁷Z. Feng, X. Tian, Z. Li, Z. Hu, Y. Zhang, X. Kang, J. Ning, Y. Zhang, C. Zhang, Q. Feng, H. Zhuo, J. Zhang, and Y. Hao, *IEEE Electron Device Letters* **41**, 333 (2020). ¹⁸A. Jayawardena, R. P. Ramamurthy, A. C. Ahyi, D. Morissette, and S. Dhar, *Applied Physics Letters* **112**, 192108 (2018), <https://doi.org/10.1063/1.5019270>.
- ¹⁹T.-H. Hung, K. Sasaki, A. Kuramata, D. N. Nath, P. Sung Park, C. Polchinski, and S. Rajan, *Applied Physics Letters* **104**, 162106 (2014), <https://doi.org/10.1063/1.4873546>.
- ²⁰H. Zhou, S. Alghmadi, M. Si, G. Qiu, and P. D. Ye, *IEEE Electron Device Letters* **37**, 1411 (2016).
- ²¹D. Biswas, C. Joishi, J. Biswas, K. Thakar, S. Rajan, and S. Lodha, *Applied Physics Letters* **114**, 212106 (2019), <https://doi.org/10.1063/1.5089627>.
- ²²W. R. Boogaard A., Kovalgin A., *ECS transactions* **35**, 259 (2011).
- ²³C. Ozgit, I. Donmez, M. Alevli, and N. Biyikli, *Thin Solid Films* **520**, 2750 (2012).
- ²⁴H.-Y. Chen, H.-L. Lu, J.-X. Chen, F. Zhang, X.-M. Ji, W.-J. Liu, X.-F. Yang, and D. W. Zhang, *ACS Applied Materials & Interfaces* **9**, 38662 (2017), PMID: 29039913, <https://doi.org/10.1021/acsami.7b12262>.

- ²⁵K. P. McKenna and A. L. Shluger, Proceedings of the Royal Society A: Mathematical, Physical and Engineering Sciences **467**, 2043 (2011),
<https://royalsocietypublishing.org/doi/pdf/10.1098/rspa.2010.0518>.
- ²⁶D. R. Clarke, Annual Review of Materials Science **17**, 57 (1987), <https://doi.org/10.1146/annurev.ms.17.080187.000421>.
- ²⁷M. A. Bhuiyan, H. Zhou, R. Jiang, E. X. Zhang, D. M. Fleetwood, P. D. Ye, and T. Ma, IEEE Electron Device Letters **39**, 1022 (2018).

Supplementary Material

Charge trap layer enabled positive tunable V_{fb} in β -Ga₂O₃ gate stacks for enhancement mode transistors

Dipankar Biswas,¹ Chandan Joishi,^{1,2} Jayeeta Biswas,¹ Prabhans Tiwari,¹ and

Saurabh Lodha^{1,a}

*¹Department of Electrical Engineering, Indian Institute of Technology Bombay, Mumbai,
Maharashtra 400076, India*

*²Department of Electrical and Computer Engineering, The Ohio State University, Columbus, OH
43210, U.S.A.*

E-mail: slodha@ee.iitb.ac.in

^aTo whom correspondence should be addressed

Extraction of β -Ga₂O₃ substrate doping concentration using reverse-biased C-V characteristics

Background doping (N_D) of the β -Ga₂O₃ substrate used in this work has been extracted using the standard technique of reverse-biased capacitance-voltage C-V measurement. Fig. 1(a) shows the C-V characteristics of an as-fabricated Ni/Al₂O₃/SiO₂/ β -Ga₂O₃ capacitor. From the slope of the $1/C^2 - V$ plot (shown in Fig. 1(b)), obtained from the C-V data shown in Fig. 1(a), N_D has been extracted using, $N_D = 2/[q\epsilon_r\epsilon_o A^2 d(C^2)/dV]$ where, q , ϵ_r , ϵ_o and A are elementary charge, relative permittivity of β -Ga₂O₃, permittivity of vacuum and gate area, respectively.

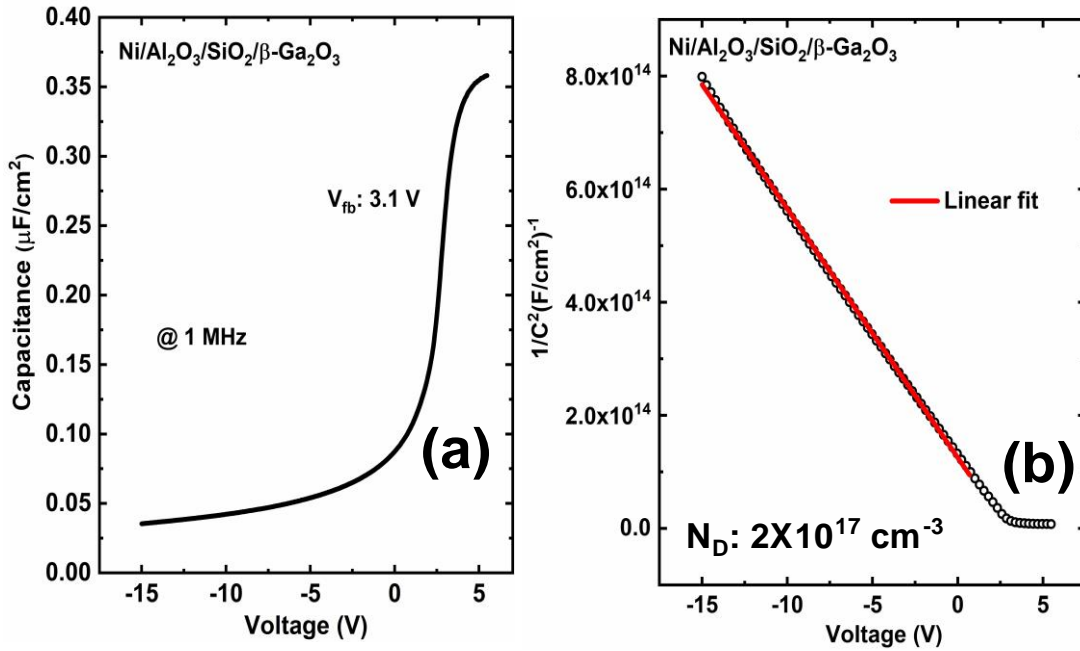


Figure 1: (a) C-V characteristics of as-fabricated Ni/Al₂O₃/SiO₂/ β -Ga₂O₃ gate stack, (b) $1/C^2 - V$ plot used to extract N_D .

Charge injection mechanism in the Ni/Al₂O₃/SiO₂/ β -Ga₂O₃ and Ni/Al₂O₃/AlN/SiO₂/ β -Ga₂O₃ gate stacks

Fig. 2(a) shows the variation in the gate current density J_g with increasing positive stress voltage applied at the gate of a Ni/Al₂O₃/AlN/SiO₂/ β -Ga₂O₃ MOSCAP. The linear dependence of $\ln J_g/E_{ox}^2$ on $1/E_{ox}$ (as shown by the red line in Fig. 2(b)) confirms F-N tunneling to be the dominant

mechanism for conduction through the gate stack beyond 6 V of gate bias.^{1,2} E_{ox} is the electric field across 4.8 nm SiO_2 .

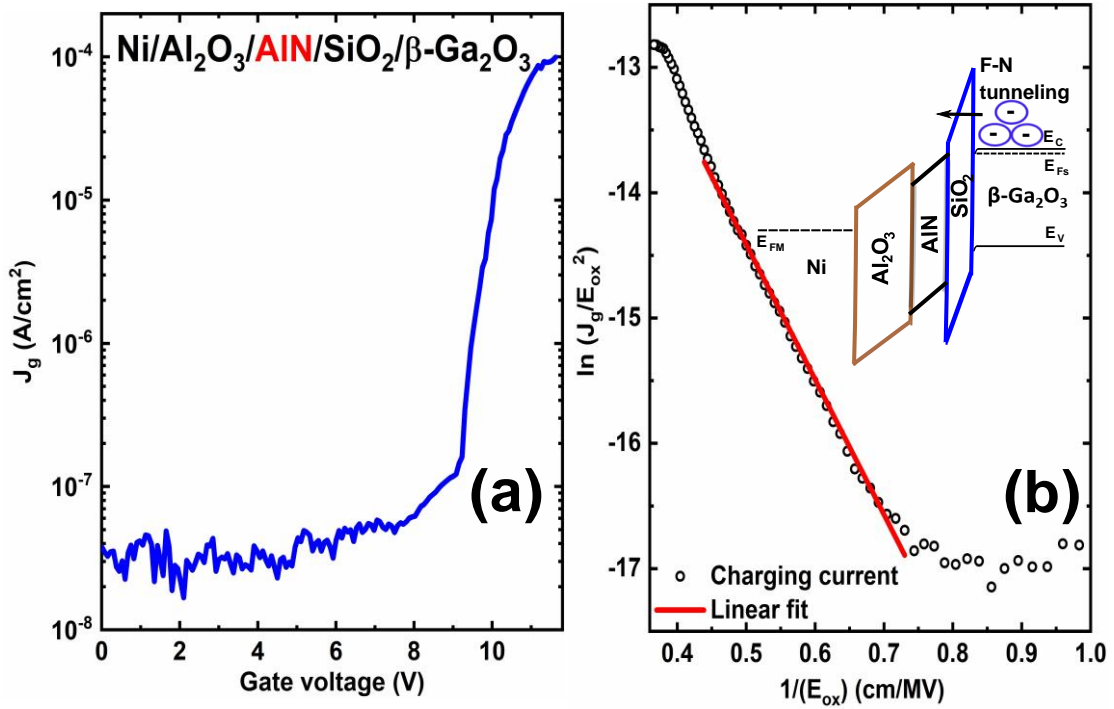


Figure 2: (a) J_g vs gate voltage for the $\text{Ni}/\text{Al}_2\text{O}_3/\text{AlN}/\text{SiO}_2/\beta\text{-Ga}_2\text{O}_3$ capacitor, (b) $\ln J_g/E_{ox}^2$ vs $1/E_{ox}$ obtained from J_g vs gate voltage shown in Fig. 2(a). The red line shows the linear dependence of $\ln J_g/E_{ox}^2$ on $1/E_{ox}$ confirming F-N tunneling to be the charge injection mechanism.

Border trap analysis and its impact on V_{fb} after charge trapping in the gate stack

Bi-directional HFCV characteristics measured at a frequency of 1 MHz (after charge trapping) highlight V_{fb} shifts of 0.1 V and 0.3 V. These lead to border trap densities of $7.1 \times 10^{11} \text{ cm}^{-2}$ and $1.6 \times 10^{12} \text{ cm}^{-2}$ for $\text{Ni}/\text{Al}_2\text{O}_3/\text{SiO}_2/\beta\text{-Ga}_2\text{O}_3$ and $\text{Ni}/\text{Al}_2\text{O}_3/\text{AlN}/\text{SiO}_2/\beta\text{-Ga}_2\text{O}_3$ gate stacks, respectively. Hence, the large positive shifts in V_{fb} along with its tunability cannot be attributed to border traps.

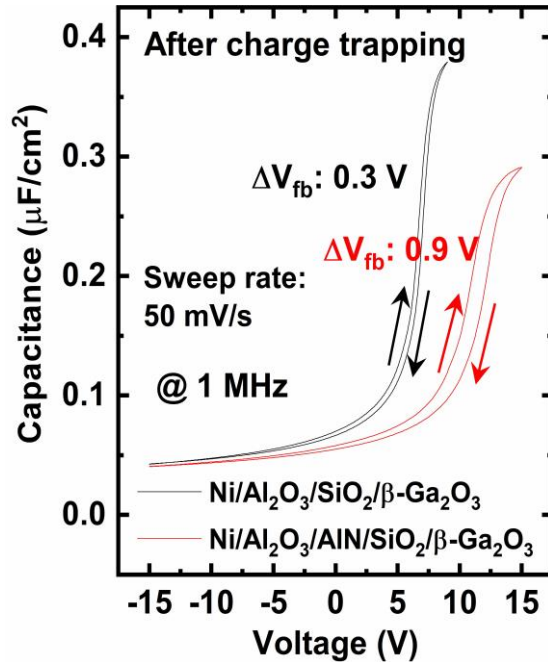


Figure 3: Bi-directional $C - V$ hysteresis data for $\text{Ni}/\text{Al}_2\text{O}_3/\text{SiO}_2/\beta\text{-Ga}_2\text{O}_3$ and $\text{Ni}/\text{Al}_2\text{O}_3/\text{AlN}/\text{SiO}_2/\beta\text{-Ga}_2\text{O}_3$ gate stacks measured after charge trapping.

XPS analysis of AlN deposited by PEALD at 200 °C

Fig. 4(a) shows the de-convoluted Al2p XPS spectrum where the main peak position of 74.41 eV confirms the presence of Al-N bonds (i.e. AlN), whereas, the sub-peak at 75.61 eV corresponds to Al-O bonds, indicating the presence of Al_xO_y (where $x < 2$, $y < 3$). This is consistent with the N1s spectrum shown in Fig. 4(b) where the presence of a main peak at 397.26 eV corresponds to Al-N bonds whereas, the main sub-peak at 398.73 eV suggests the formation of N-Al-O bonds (i.e. AlON). A lower energy sub-peak at 395.77 eV is due to N-N bonds. The atomic percentages extracted from the areas under the Al2p, N1s and O1s (Fig. 4(c)) spectra show a distribution of 39.3%, 35.9% and 24.7% for Al, N and O in the deposited AlN film.^{3,4}

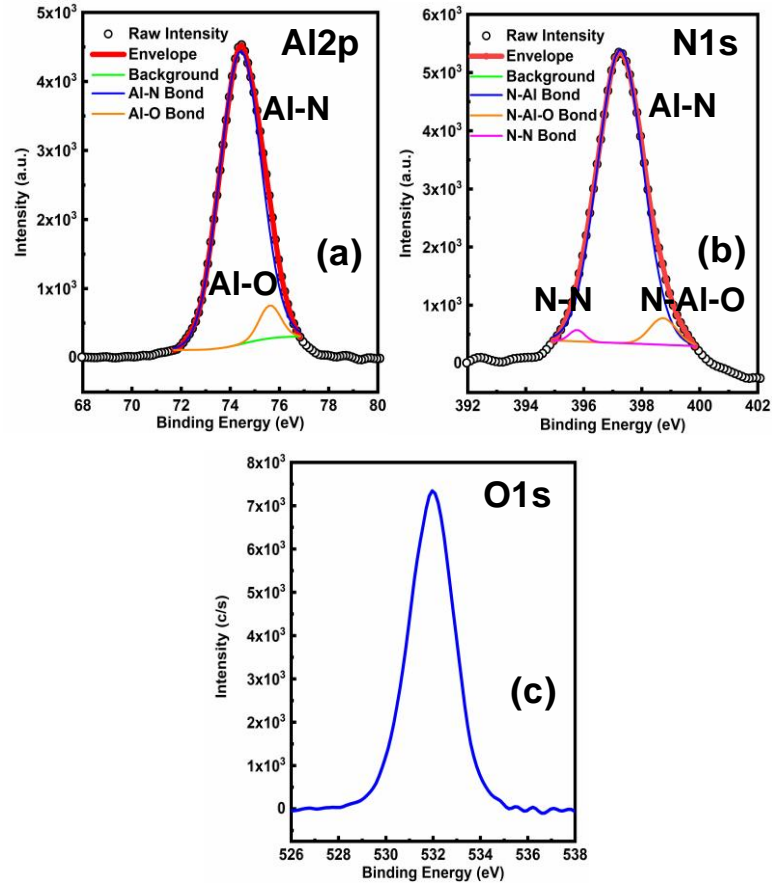


Figure 4: (a) Al₂p, (b) N₁s and (c) O₁s XPS spectra of AlN dielectric.

To verify the formation of Al₂O₃/SiO₂ and Al₂O₃/AlN/SiO₂ stacks on β -Ga₂O₃, XPS depth profile measurements were performed on Si monitor wafers (loaded in the ALD chamber during gate dielectric stack deposition on β -Ga₂O₃). Figs. 5(a) and (b) show the depth profiles of Al₂O₃ (12 nm)/SiO₂ (4.8 nm) and Al₂O₃ (12 nm)/AlN (5 nm)/SiO₂ (4.8 nm) dielectric stacks on Si, respectively. The presence of AlN (AlON) between 12 nm Al₂O₃ and 4.8 nm SiO₂ has been highlighted in Fig. 5(b).

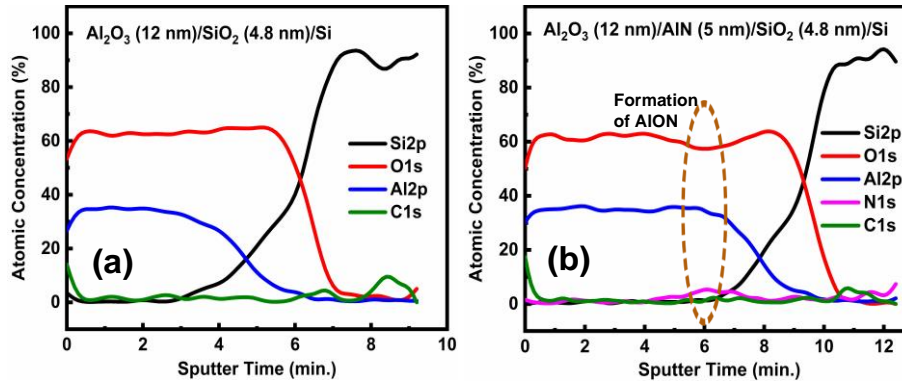


Figure 5: XPS depth profiles of (a) Al₂O₃/SiO₂/Si and (b) Al₂O₃/AlN/SiO₂/Si stacks.

References

- (1) Kamimura, T.; Sasaki, K.; Hoi Wong, M.; Krishnamurthy, D.; Kuramata, A.; Masui, T.; Yamakoshi, S.; Higashiwaki, M. Band alignment and electrical properties of Al₂O₃/Ga₂O₃ heterojunctions. *Applied Physics Letters* 2014, *104*, 192104.
- (2) Jayawardena, A.; Ramamurthy, R. P.; Ahyi, A. C.; Morissette, D.; Dhar, S. Interface trapping in (201) Ga₂O₃ MOS capacitors with deposited dielectrics. *Applied Physics Letters* 2018, *112*, 192108.
- (3) Chen, H.-Y.; Lu, H.-L.; Chen, J.-X.; Zhang, F.; Ji, X.-M.; Liu, W.-J.; Yang, X.-F.; Zhang, D. W. Low-Temperature One-Step Growth of AlON Thin Films with Homogenous Nitrogen-Doping Profile by Plasma-Enhanced Atomic Layer Deposition. *ACS Applied Materials & Interfaces* 2017, *9*, 38662–38669, PMID: 29039913.
- (4) McKenna, K. P.; Shluger, A. L. Electron and hole trapping in polycrystalline metal oxide materials. *Proceedings of the Royal Society A: Mathematical, Physical and Engineering Sciences* 2011, *467*, 2043–2053.